nature nanotechnology

LETTERS

PUBLISHED ONLINE: 15 MAY 2017 | DOI: 10.1038/NNANO.2017.86

Energy-dependent path of dissipation in nanomechanical resonators

Johannes Güttinger[1], Adrien Noury[1], Peter Weber[1], Axel Martin Eriksson[2], Camille Lagoin[1], Joel Moser[1], Christopher Eichler[3], Andreas Wallraff[3], Andreas Isacsson[2] and Adrian Bachtold[1]*

Energy decay plays a central role in a wide range of phenomena[1–3], such as optical emission, nuclear fission, and dissipation in quantum systems. Energy decay is usually described as a system leaking energy irreversibly into an environmental bath. Here, we report on energy decay measurements in nanomechanical systems based on multilayer graphene that cannot be explained by the paradigm of a system directly coupled to a bath. As the energy of a vibrational mode freely decays, the rate of energy decay changes abruptly to a lower value. This finding can be explained by a model where the measured mode hybridizes with other modes of the resonator at high energy. Below a threshold energy, modes are decoupled, resulting in comparatively low decay rates and giant quality factors exceeding 1 million. Our work opens up new possibilities to manipulate vibrational states[4–7], engineer hybrid states with mechanical modes at completely different frequencies, and to study the collective motion of this highly tunable system.

Energy decay is central in many fields of physics, including acoustics[1], non-equilibrium thermodynamics[2] and the quantum mechanics of dissipative systems[3]. A dissipative system is typically assumed to be coupled to a given thermal environmental bath. The rate of the coupling is often considered to be independent of the system energy. Recently, nonlinear phenomena associated with dissipation have attracted considerable interest. These include measurements on radio-frequency superconducting resonators, where the energy-dependent decay rate is attributed to the saturation of two-level defect states[8]. In addition, measurements on nanomechanical resonators have been described by a phenomenological nonlinear decay process[9–13]. However, the physical mechanism responsible for the nonlinear dissipation remains elusive. Understanding the origin of dissipation in mechanical resonators is crucial[14–18], because it is a key figure of merit for many applications, such as mass, force and spin sensing[19–22]. Here, we report energy decay measurements on mechanical resonators that are radically different from what is usually observed, and that allow us to reveal the nature of the nonlinear energy decay process.

We first recall the way by which energy stored in a vibrating guitar string is dissipated. In essence, the sound coming from the guitar originates from the coupling of the vibrating string with the air in the room, which acts as the environmental bath. To increase the intensity of the sound, and to quickly tone the sound down, the string is coupled resonantly to some cavity modes of the guitar body. As the string and these cavity modes vibrate at similar frequencies, the vibrational energy is transferred efficiently. The coupling is said to be linear, in a sense that the coupling energy H_c is proportional to the product of the vibration amplitude of the string q_1 by the vibration amplitude q_2 of the guitar body, $H_c \propto q_1 q_2$. For strongly coupled modes, hybridization occurs, and the two modes decay in unison with an average decay rate $(\gamma_1 + \gamma_2)/2$. However, when the coupling is weak, the two modes are decoupled and decay with rates γ_1 and γ_2, respectively.

In this Letter, we consider the case where the coupling between modes is nonlinear, and we show that this results in nonlinear energy decay processes in graphene resonators. Nonlinear couplings have the peculiarity of enabling energy transfer between vibrational modes even if resonant frequencies are far apart. For this to happen, the ratio of resonant frequencies ω_2/ω_1 has to be close to an integer n (refs 23,24). Although the modes are in the classical regime, this nonlinear mode coupling can be easily understood by considering the energy ladders of harmonic oscillators. Figure 1a illustrates an energy conserving process (here $n = 3$) annihilating simultaneously three quanta in mode 1, while creating one quantum in mode 2. The lowest-order nonlinear coupling term in the Hamiltonian that can achieve this exchange is $H_c \propto q_1^3 q_2$. Nonlinear coupling is particular, as the coupling strength is energy dependent. At high vibrational amplitude, the modes hybridize, and decay in unison. At low amplitude, the coupling strength is weak, so that the two modes are decoupled and decay with rates γ_1 and γ_2, respectively (Fig. 1b). As a result, the flow of energy takes different paths during an energy decay measurement of mode 1. At high amplitude, the energy of the vibrations is transferred into the bath of mode 1 directly, and into the vibrations and the bath of mode 2. At low amplitude, the dissipation channel to the bath of mode 2 is closed. This abrupt variation of the mechanical decay has to our knowledge neither been predicted nor been measured. The associated nonlinear energy decay process is generic and should be relevant to a large variety of systems, such as mechanical, optical and electrical resonators.

Graphene-based resonators are well suited for observing such a nonlinear energy decay process (Fig. 1c,d). Indeed, their resonant frequencies can be widely tuned by electrostatic means[6,7,9,25–28] allowing us to set the frequency ratio of two modes to an integer.

Energy decay measurements are carried out by preparing the resonator in an out-of-equilibrium state using a capacitive driving force, then switching the drive off and measuring the vibrational amplitude as the mechanical energy freely decays (Fig. 2a). A circular graphene mechanical resonator is capacitively coupled to a superconducting microwave cavity to detect the mechanical vibrations with a short time resolution, a high displacement sensitivity and over a broad range of vibrational amplitudes[29–32]. The time resolution is limited by the inverse of the coupling rate of the cavity to the external readout circuit, which is of the order of $\kappa_{ext}/2\pi \approx 1$ MHz in our devices. High displacement sensitivity with minimal heating is demonstrated by resolving thermal

[1]ICFO-Institut de Ciencies Fotoniques, The Barcelona Institute of Science and Technology, 08860 Castelldefels (Barcelona), Spain. [2]Department of Physics, Chalmers University of Technology, SE-412 96 Göteborg, Sweden. [3]Department of Physics, ETH Zürich, CH-8093 Zürich, Switzerland.
*e-mail: adrian.bachtold@icfo.es

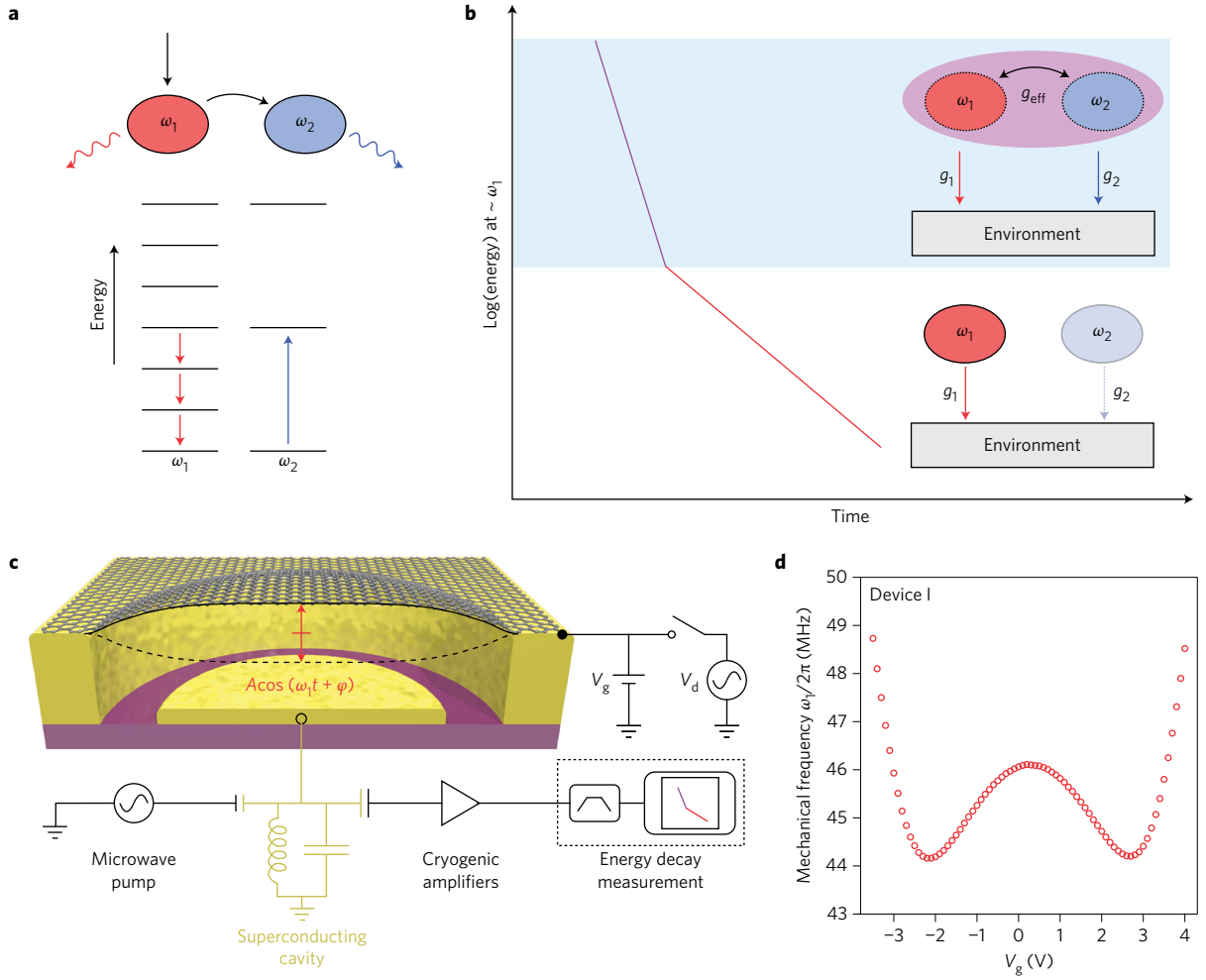

Figure 1 | Nonlinear energy decay process, mode hybridization and graphene resonator. a, Energy diagram showing an energy exchange process between two harmonic oscillators. In the top part, we depict the flow of energy when driving mode 1 strongly. **b**, Energy decay measured at the frequency of mode 1. Because of the nonlinearity, the effective coupling strength depends on energy. At high energy, the modes are hybridized and decay in unison. As energy decays, the modes decouple, resulting in a change of the decay rate for mode 1. **c**, Measurement set-up with schematic cross-section of a circular graphene drum vibrating as cos ($\omega_1 t + \varphi$), where φ is the phase relative to the capacitive driving force. The motion is detected with the superconducting microwave cavity. After cryogenic amplification, the output signal of the cavity is recorded and digitally computed to obtain the energy and the frequency of the vibrations as a function of time. The application of the static gate voltage V_g between the graphene drum and the cavity electrode allows the mechanical resonance frequencies to be tuned; the oscillating voltage V_d is used to drive the resonator. **d**, Frequency of the fundamental mode as a function of gate voltage V_g.

motion at about 50 mK, corresponding to ≈25 quanta of vibrations. The displacement sensitivity can be further improved using a near quantum-limited Josephson parametric amplifier (JPA) for the readout of devices with comparatively low signal output[33]. We typically record vibrations with amplitudes ranging from 1 pm to 1 nm. Using a time-resolved acquisition scheme combined with real-time digital signal processing (dashed box in Fig. 1c), we record the two quadratures of motion, which are digitally squared to compute the vibrational energy. Energy decay traces are obtained by averaging typically 1,000 measurements and subtracting a time-independent noise background that is related to the amplifier chain. Decay traces are displayed as vibration amplitude versus time to make contact with other experiments. All the data presented here are taken at 15 mK. See Supplementary Sections 1–5 for further details on the devices, the measurement set-up and the displacement calibration.

In the low-amplitude regime, this measurement scheme is beneficial as it allows us to observe record-high quality factors (Fig. 2b). The measured vibration amplitude of the fundamental mode at frequency ω_1 decays exponentially in time as $\propto e^{-\gamma_1 t/2}$ with an energy decay rate $\gamma_1 \approx 1/(3.6\ \text{ms})$. This corresponds to a quality factor Q exceeding 1 million, surpassing previously reported Q-factors in graphene[9,29,31]. By collecting energy decay traces using different drive frequencies near ω_1, we show that the Q-factor is independent of the drive frequency and the vibrational amplitude at the beginning of the ring-down (Fig. 2b). One reason for the observation of such high Q-factors is the fact that our technique is immune from dephasing, in contrast to previous spectral measurements on graphene resonators. Comparing energy decay measurements with spectral thermal motion measurements reveals that dephasing is significant, as the resonance linewidth is more than twice as large as the energy decay rate (Supplementary Section 6).

In the high-amplitude regime, our high-precision measurements reveal a crossover in the energy decay rate during the ring-down (Fig. 3a,b). This finding is robust, since it is observed in all the studied resonators. Changing the amplitude and frequency of the initial driving force does not affect the rates and amplitudes associated with the crossovers. However, what strongly affects the energy decay traces is the static voltage V_g applied between the graphene

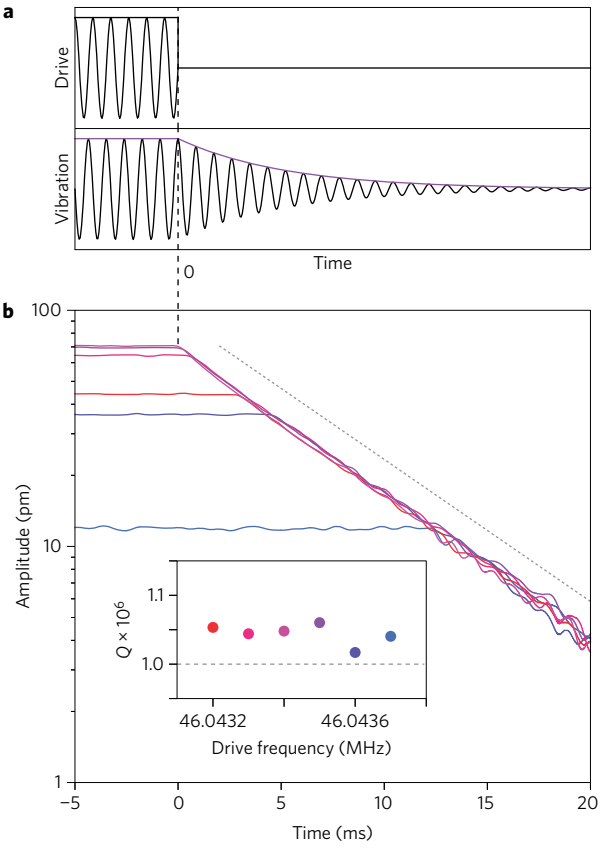

Figure 2 | Energy decay measurements of a graphene resonator with a *Q*-factor of 1 million in the low-vibrational-amplitude regime. **a**, Measurement principle. At time $t = 0$, the mechanical driving force is switched off and the vibrational amplitude starts to decay. **b**, Measured energy decay of the vibrational amplitude of device I as a function of time for different drive frequencies (see colours in inset). The graphene membrane is 5 to 6 layers thick, as characterized by optical contrast measurements (Supplementary Section 4). The lower-amplitude traces are shifted in time so all decaying curves overlap. The dashed grey line indicates an exponential decay corresponding to a *Q*-factor of 1 million. The inset shows the quality factor as a function of drive frequency. We apply $V_g = 0.6$ V and pump the cavity with $n_p \approx 1{,}000$ photons.

resonator and the cavity (Fig. 3a,b). This is a first indication that the crossover of the decay is related to nonlinear mode coupling, since the variation of V_g strongly modifies the different resonant frequencies. To ensure that all the vibrational energy during the decay is properly captured, we use signal filtering with large bandwidth. This is because the frequency changes during the decay (Fig. 3c). On comparing this smooth frequency change and the vibrational amplitude decay, we get the expected quadratic amplitude dependence of the frequency related to the nonlinear Duffing restoring force[34] (Fig. 3d and Supplementary Section 7).

We characterize mode coupling by measuring the response of the fundamental mode to the driving force. For this, we tune V_g so the frequency ω_1 of the fundamental mode is about one third the frequency ω_2 of a higher-order mode, that is, $\omega_1/2\pi = 44.132$ MHz and $\omega_2/2\pi = 132.25$ MHz. For intermediate drive amplitudes V_d, the response of mode 1 is that of a Duffing resonator with a softening nonlinearity (Fig. 4a). However, as driving increases, we observe a saturation of the frequency at which the high-amplitude state switches to the low-amplitude state. The related bifurcation points are shown in the top part of Fig. 4a. This saturation of the frequency is due to the efficient energy transfer between mode 1 and mode 2 when the frequency ratio is an integer[23]. Driving the system even harder, the response exhibits a plateau behaviour as shown in Fig. 4b.

We now show that the change in decay rate is related to nonlinear mode coupling. To demonstrate this, we use the driven response measurements shown above to determine the parameters of a minimal model of coupled nonlinear resonators, which allows us to describe the measured energy decay with good accuracy, as discussed next. Both features, frequency saturation and plateau, are well reproduced by two coupled nonlinear modes

$$\ddot{q}_1 = -\omega_1^2 q_1 - \gamma_1 \dot{q}_1 - \alpha_1 q_1^3 - m^{-1}\partial H_c/\partial q_1 + aV_d \quad (1)$$

$$\ddot{q}_2 = -\omega_2^2 q_2 - \gamma_2 \dot{q}_2 - \alpha_2 q_2^3 - m^{-1}\partial H_c/\partial q_2 \quad (2)$$

with α_1 and α_2 the Duffing constants, and a the force constant. The interaction Hamiltonian is $H_c = mgq_1^3 q_2$ with $m \approx 60$ fg the effective mass of mode 1 and g the coupling constant (Supplementary Section 4). The displacement q_2 of mode 2 is normalized to have the same effective mass. In these equations we only include terms necessary to capture the essential physics. We thus omit higher-order restoring force terms, off-resonant interaction terms and purely dispersive coupling terms. Although the omitted terms may give a better fit, we seek for clarity to minimize the number of free parameters. As can be seen from Fig. 4a–c, the model allows us to describe the measurements of the response and the reduced bifurcation diagram with good agreement (Supplementary Section 8). Remarkably, the parameters used to fit these driven measurements reproduce quantitatively the measured energy decay trace (Fig. 4d). This shows that nonlinear mode coupling is at the origin of the observed crossover in the decay rate. Note that single energy decay traces are expected to feature oscillations because of mode coupling (Fig. 4e). But our simulations show that these oscillations disappear when averaging multiple traces, in agreement with our experiments. For the strong drives used for the excitation of the resonator, mechanical nonlinearities cause the initial state to be different from one decay measurement to the next, so that the oscillations in the averaged decay trace are washed out. We find that the averaged decay trace is approximately described by two exponential decays. The decay rate crossovers from about $(\gamma_1 + \gamma_2)/2$ to γ_1.

The change in the decay rate is related to the crossover from mode hybridization to weak mode coupling as the vibration amplitude freely decays. Indeed, the measured crossover amplitude of $\sim$200 pm is consistent with the $\sim$300 pm obtained from the crude estimate $g_{\mathrm{eff}}^2 \sim (\gamma_1 - \gamma_2)^2/4 + \delta_{\mathrm{eff}}^2$. Here, $g_{\mathrm{eff}} = gm\omega_1^2 A_1^2/2$ is the rate of energy exchange between the two modes with A_1 the amplitude of mode 1; and δ_{eff} is the offset of frequency between the two modes including Duffing shifts (Supplementary Section 8.4). During the ringdown, the crossover between different energy decay rates is controlled primarily by the variation of g_{eff}, and only weakly by the shift of δ_{eff}. In the opposite case, the modes would be either decoupled or hybridized at the beginning of the ringdown depending on the initial value of δ_{eff}. This is not observed in our experiments, since the decay rate is larger at the beginning of the ringdown irrespective of the initial δ_{eff}. This indicates that the crossover is related to the variation of g_{eff}. The nonlinear behaviour in our energy decay measurements cannot be related to the Velcro effect[35], where the total energy of the resonator, which is typically 0.1–1 eV at the lowest-amplitude crossover, is used to break surface bonds between the graphene flake and the supporting electrodes. Indeed, the release of the total energy from the mechanical resonator would then result in a dramatic reduction of the vibrational amplitude, but this is not observed in our experiments. Furthermore, our experimental finding is not related to the coupling of the resonator to two-level defect states[8], which become saturated

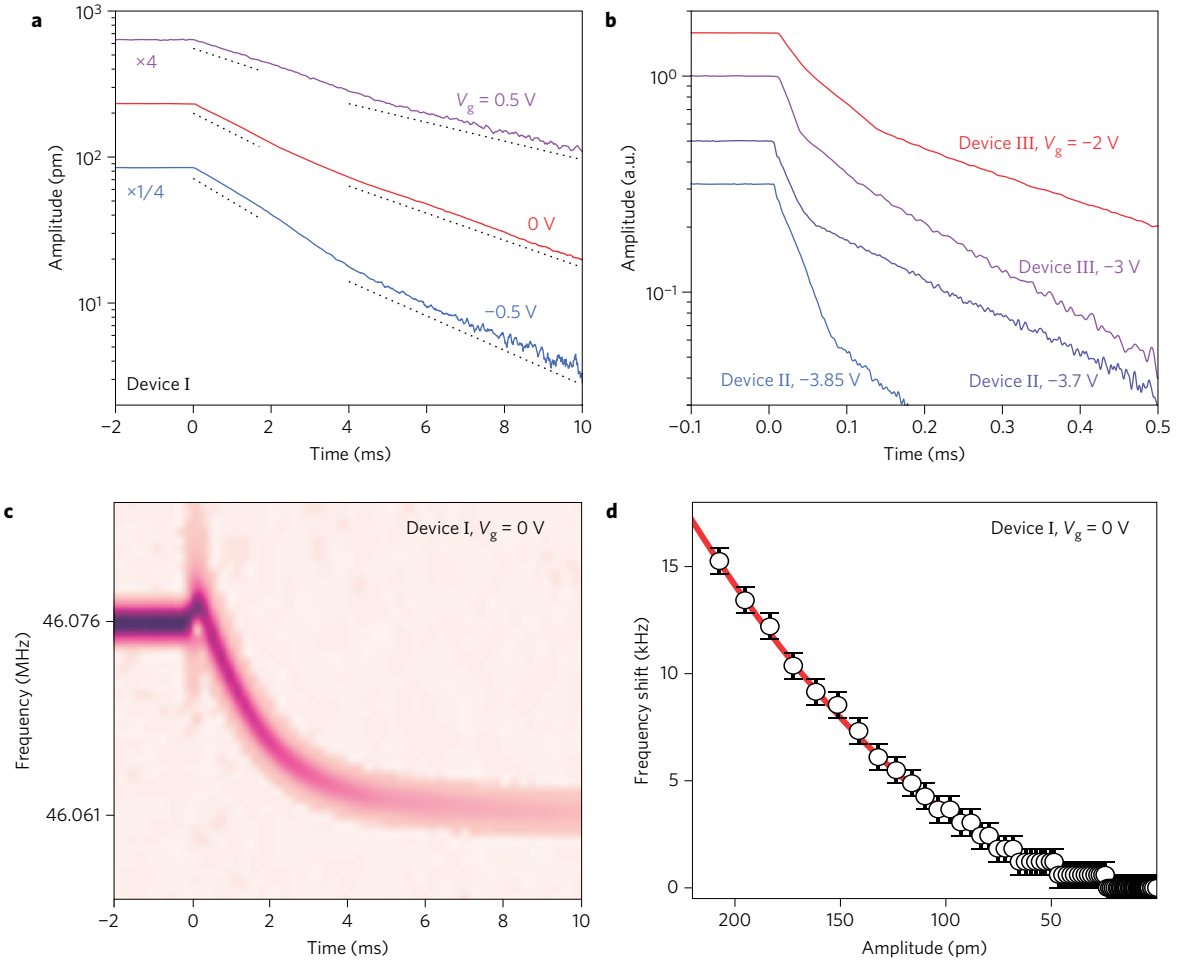

Figure 3 | Energy decay in the high-vibrational-amplitude regime. a,**b**, Energy decay measurements at different V_g for three different devices (labeled I, II and III). In all cases, the decay rate changes abruptly. The bandwidth of the bandpass filter in **a** is 150 kHz for the violet and red traces and 200 kHz for the blue trace. The dashed lines in **a** indicate the slopes in the low and high amplitude regimes. The amplitude of the violet and the blue traces are multiplied by 4 and 1/4, respectively. In **b**, the bandwidth is 400 kHz and 200 kHz for devices II and III, respectively. **c**, Time dependence of the short-time Fourier transform of the vibrations corresponding to the red amplitude decay trace in **a**. **d**, Frequency shift as a function of vibrational amplitude. The quadratic dependence (red line) is in agreement with the frequency pulling expected from the nonlinear restoring force at low vibration amplitude.

at high vibration amplitudes. Indeed, such a coupling would lead to a reduction of the decay rate as the vibrational amplitude increases, which is the opposite of the measured behaviour.

The coupling constant g obtained from our simulations is in reasonable agreement with the value expected from continuum elasticity. In the case of a circular membrane clamped at the circumference, the strength of the fourth-order coupling expected from continuum elasticity yields $mg \sim NE_{2d}/R^2$ with a prefactor that depends on the shape of the modes[36]. Using $N = 35$ as the layer number of the graphene flake in device II, $E_{2d} = 340\ \mathrm{N\ m^{-1}}$ the two-dimensional Young modulus of graphene, $R = 1.6\ \mu\mathrm{m}$ the radius of the resonator, and $mg = 7 \times 10^{16}\ \mathrm{J\ m^{-4}}$ the coupling obtained from our simulations, we get a reasonable prefactor of 14 (ref. 36). The nonlinear constant α_1 deduced from our simulations is consistent with the value of a graphene flake that is slightly bent by the static capacitive force[29]. All the parameters of the coupled system in Fig. 4 can be found in Supplementary Section 8.2. We note that these parameters change when sweeping the gate voltage.

The mode frequency ratio does not need to be strictly an integer to observe the crossover in the decay rate. The crossover is indeed measured when detuning V_g so that $\omega_2 \neq 3\omega_1$ (Supplementary Section 7). However, the hybridization occurs at larger amplitudes (Fig. 4f). Energy decay traces with crossover can be measured in different V_g ranges, indicating that the frequency ratio of the mode coupling is close to an integer that can be different from three. Clear signatures of internal resonance in energy-decay and spectral measurements are observed with the gate voltage set at −3.88, −3.78 and −3.3 V.

In summary, we reveal how nonlinear mode coupling can drastically change the dynamics of energy dissipation in nanomechanical resonators, that is, by enhancing dissipation at high vibration amplitude via mode hybridization. This effect is not a curiosity limited to a restrained parameter space, as the effect of hybridization is observed here for vibration amplitudes as low as ~100 pm, while graphene and nanotube resonators are driven to the 1–10 nm amplitude range in many experiments. It will be intriguing to investigate hybridization driven by thermal noise. For this, nanotube resonators are appealing[22,37], since the variance of thermal vibrations can be well above $(1\ \mathrm{nm})^2$ at room temperature. It will be exciting to hybridize three and more modes, since this collective motion will feature rich physics with the interplay of hybridization, Duffing nonlinearity and noise. Hybridization of multiple modes could be achieved with membrane resonators of various shapes whose modes are tunable using a combination of split gates[6]. In addition, hybridization opens up new possibilities to control

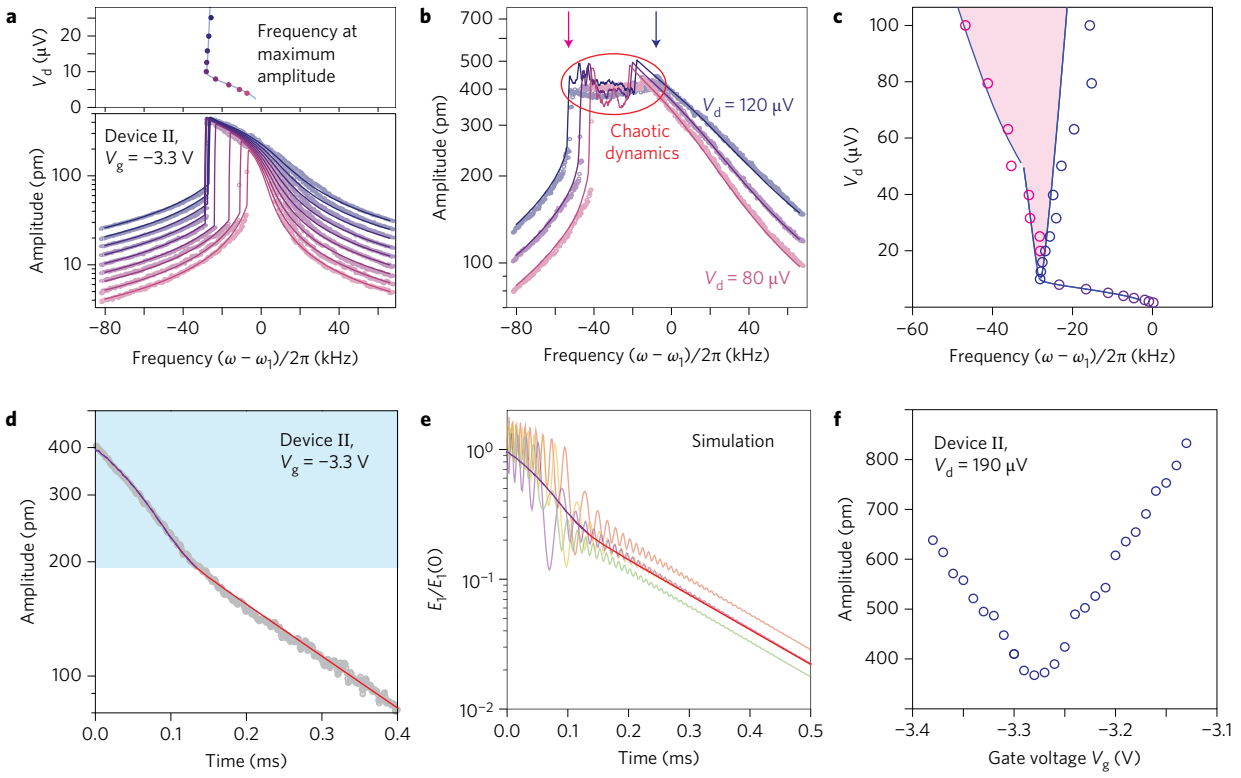

Figure 4 | Driven response and energy decay traces. a, Measured and simulated driven response of the fundamental mode for intermediate drive strengths (bottom), the corresponding measured and calculated bifurcations where the high-amplitude states switch to the low-amplitude states (top). The drive is swept from high frequency to low frequency. The observed saturation of the switching frequency at high drive occurs when $\omega_2 = 3\omega_1$, providing strong evidence for mode interaction. **b**, Measured and simulated driven response of the fundamental mode for strong driving. In simulations, the plateau is associated with chaotic dynamics of coupled nonlinear modes. The blue and pink arrows indicate the location of the experimentally detectable bifurcations in this regime with a downward frequency sweep. **c**, Reduced bifurcation diagram showing the experimentally accessible bifurcations (measured and calculated) for a downward frequency sweep. The data points are obtained from driven response measurements at different drive strengths; see **a**,**b**. A more complete diagram can be found in Supplementary Section 8.1. The pink region corresponds to driven responses that exhibit a plateau behaviour. **d**, Measured and simulated energy decay traces. Using the same parameters as in the fits in **a**–**c**, the model satisfactorily reproduces the measured energy decay trace, including the crossover in the decay rate. The grey points correspond to measurements and the violet and red lines to simulations. **e**, Simulated individual energy decay traces revealing coherent oscillations. Different traces correspond to different initial states, which are all prepared with the same drive strength. The calculated trace in **d** is obtained from averaging over many ring-downs. **f**, Vibration amplitude of the plateau feature in **b** as a function of gate voltage V_g. The plateau is a consequence of mode hybridization (Supplementary Section 8.1). The amplitude is extracted from the measured response at the frequency just below the bifurcation indicated by the blue arrow in **b**.

dissipation by electrostatic means and to manipulate vibrational states coherently[4–7].

When preparing the manuscript, we learned about another work on the role of nonlinear mode coupling in the dissipation of mechanical resonators[38].

Data availability. The data that support the plots within this paper and other findings of this study are available from the corresponding author upon reasonable request.

Received 29 September 2016; accepted 30 March 2017; published online 15 May 2017

References

1. Rayleigh, J. W. Some general theorems relating to vibrations. *Proc. London Math. Soc.* **s1–4,** 357–368 (1871).
2. Onsager, L. Reciprocal relations in irreversible processes. I. *Phys. Rev.* **37,** 405–426 (1931).
3. Caldeira, A. O. & Leggett, A. J. Path integral approach to quantum Brownian motion. *Physica* **121A,** 587–616 (1983).
4. Faust, T., Rieger, J., Seitner, M. J., Kotthaus, J. P. & Weig, E. M. Coherent control of a classical nanomechanical two-level system. *Nat. Phys.* **9,** 485–488 (2013).
5. Okamoto, H. *et al.* Coherent phonon manipulation in coupled mechanical resonators. *Nat. Phys.* **9,** 480–484 (2013).
6. De Alba, R. *et al.* Tunable phonon–cavity coupling in graphene membranes. *Nat. Nanotech.* **11,** 741–746 (2016).
7. Mathew, J. P., Patel, R. N., Borah, A., Vijay, R. & Deshmukh, M. M. Dynamical strong coupling and parametric amplification of mechanical modes of graphene drums. *Nat. Nanotech.* **11,** 747–751 (2016).
8. Gao, J., Zmuidzinas, J., Mazin, B. A., LeDuc, H. G. & Day, P. K. Noise properties of superconducting coplanar waveguide microwave resonators. *Appl. Phys. Lett.* **90,** 102507 (2007).
9. Eichler, A. *et al.* Nonlinear damping in mechanical resonators made from carbon nanotubes and graphene. *Nat. Nanotech.* **6,** 339–342 (2011).
10. Zaitsev, S., Shtempluck, O., Buks, E. & Gottlieb, O. Nonlinear damping in a micromechanical oscillator. *Nonlinear Dynamics* **67,** 859–883 (2012).
11. Imboden, M., Williams, O. A. & Mohanty, P. Observation of nonlinear dissipation in piezoresistive diamond nanomechanical resonators by heterodyne down-mixing. *Nano Lett.* **13,** 4014–4019 (2013).
12. Mahboob, I. *et al.* Dispersive and dissipative coupling in a micromechanical resonator embedded with a nanomechanical resonator. *Nano Lett.* **15,** 2312–2317 (2015).
13. Polunin, P. M., Yang, Y., Dykman, M. I., Kenny, T. W. & Shaw, S. W. Characterization of MEMS resonator nonlinearities using the ringdown response. *J. Microelectromech. Sys.* **25,** 297–303 (2016).
14. Dykman, M. I. & Krivoglaz, M. A. Theory of nonlinear oscillator interacting with a medium. *Sov. Phys. Rev.* **5,** 265–442 (1984).
15. Wilson-Rae, I. Intrinsic dissipation in nanomechanical resonators due to phonon tunneling. *Phys. Rev. B* **77,** 245418 (2008).

16. Rieger, J., Isacsson, A., Seitner, M. J., Kotthaus, J. P. & Weig, E. M. Energy losses of nanomechanical resonators induced by atomic force microscopy-controlled mechanical impedance mismatching. *Nat. Commun.* **5,** 3345 (2014).
17. Tao, Y., Boss, J. M., Moores, B. A. & Degen, C. L. Single-crystal diamond nanomechanical resonators with quality factors exceeding one million. *Nat. Commun.* **5,** 3638 (2014).
18. Midtvedt, D., Croy, A., Isacsson, A., Qi, Z. & Park, H. Fermi-Pasta-Ulam physics with nanomechanical graphene resonators: intrinsic relaxation and thermalization from flexural mode coupling. *Phys. Rev. Lett.* **112,** 145503 (2014).
19. Gil-Santos, E. *et al.* Nanomechanical mass sensing and stiffness spectrometry based on two-dimensional vibrations of resonant nanowires. *Nat. Nanotech.* **5,** 641–645 (2010).
20. Hanay, M. S. *et al.* Single-protein nanomechanical mass spectrometry in real time. *Nat. Nanotech.* **7,** 602–608 (2012).
21. Chaste, J. *et al.* A nanomechanical mass sensor with yoctogram resolution. *Nat. Nanotech.* **7,** 301–304 (2012).
22. Moser, J., Eichler, A., Güttinger, J., Dykman, M. I. & Bachtold, A. Nanotube mechanical resonators with quality factors of up to 5 million. *Nat. Nanotech.* **9,** 1007–1011 (2014).
23. Antonio, D., Zanette, D. H. & Lopez, D. Frequency stabilization in nonlinear micromechanical oscillators. *Nat. Commun.* **3,** 806 (2012).
24. Eichler, A., del Álamo Ruiz, M., Plaza, J. A. & Bachtold, A. Strong coupling between mechanical modes in a nanotube resonator. *Phys. Rev. Lett.* **109,** 025503 (2012).
25. Chen, C. *et al.* Performance of monolayer graphene nanomechanical resonators with electrical readout. *Nat. Nanotech.* **4,** 861–867 (2009).
26. Singh, V. *et al.* Probing thermal expansion of graphene and modal dispersion at low-temperature using graphene nanoelectromechanical systems resonators. *Nanotechnology* **21,** 165204 (2010).
27. Barton, R. A. *et al.* Photothermal self-oscillation and laser cooling of graphene optomechanical systems. *Nano Lett.* **12,** 4681–4686 (2012).
28. Miao, T., Yeom, S., Wang, P., Standley, B. & Bockrath, M. Graphene nanoelectromechanical systems as stochastic-frequency oscillators. *Nano Lett.* **14,** 2982–2987 (2014).
29. Weber, P., Güttinger, J., Tsioutsios, I., Chang, D. E. & Bachtold, A. Coupling graphene mechanical resonators to superconducting microwave cavities. *Nano Lett.* **14,** 2854–2860 (2014).
30. Song, X., Oksanen, M., Li, J., Hakonen, P. J. & Sillanpää, M. A. Graphene optomechanics realized at microwave frequencies. *Phys. Rev. Lett.* **113,** 027404 (2014).
31. Singh, V. *et al.* Optomechanical coupling between a graphene mechanical resonator and a superconducting microwave cavity. *Nat. Nanotech.* **9,** 820–824 (2014).
32. Weber, P., Güttinger, J., Noury, A., Vergara-Cruz, J. & Bachtold, A. Force sensitivity of multilayer graphene optomechanical devices. *Nat. Commun.* **7,** 12496 (2016).
33. Eichler, C., Salathe, Y., Mlynek, J., Schmidt, S. & Wallraff, A. Quantum-limited amplification and entanglement in coupled nonlinear resonators. *Phys. Rev. Lett.* **113,** 110502 (2014).
34. Lifshitz, R. & Cross, M. Nonlinear dynamics of nanomechanical and micromechanical resonators. *Rev. Nonlinear Dyn. Complex.* **1,** 1–48 (2008).
35. Seoánez, C., Guinea, F. & Castro Neto, A. H. Dissipation in graphene and nanotube resonators. *Phys. Rev. B* **76,** 125427 (2007).
36. Eriksson, A. M., Midtvedt, D., Croy, A. & Isacsson, A. Frequency tuning, nonlinearities and mode coupling in circular mechanical graphene resonators. *Nanotechnology* **24,** 395702 (2013).
37. Benyamini, A., Hamo, A., Kusminskiy, S. V., von Oppen, F. & Ilani, S. Real-space tailoring of the electron–phonon coupling in ultraclean nanotube mechanical resonators. *Nat. Phys.* **10,** 151–156 (2014).
38. Shoshani, O., Shaw, S. W. & Dykman, M. I. Anomalous dissipation of nanomechanical modes going through nonlinear resonance. Preprint at https://arxiv.org/abs/1702.00769 (2017).

Acknowledgements

We thank M. Dykman, S. Shaw, D. Lopez, F. Guinea and N. Noury for discussions. We acknowledge G. Ceballos and the ICFO mechanical and electronic workshop for support. We acknowledge financial support by the ERC starting grant 279278 (CarbonNEMS), the EU Graphene Flagship (contract no. 604391), the Foundation Cellex, Severo Ochoa (SEV-2015-0522) and grant MAT2012-31338 of MINECO, the Fondo Europeo de Desarrollo Regional (FEDER), and the Generalitat through AGAUR. A.I. and A.M.E. acknowledge financial support through the Swedish Research Council and the Knut and Alice Wallenberg foundation.

Author contributions

P.W. fabricated the devices. J.G., A.N. and P.W. carried out the experiment with support from C.L. and J.M. Theoretical modelling and simulations were done by A.M.E. and A.I. The JPA was provided by C.E. and A.W. The data analysis was done by J.G., A.N., P.W., A.M.E., A.I. and A.B. J.G., A.I. and A.B. wrote the manuscript with comments from the other authors. A.B. supervised the work.

Additional information

Supplementary information is available in the online version of the paper. Reprints and permissions information is available online at www.nature.com/reprints. Publisher's note: Springer Nature remains neutral with regard to jurisdictional claims in published maps and institutional affiliations. Correspondence and requests for materials should be addressed to A.B.

Competing financial interests

The authors declare no competing financial interests.